Spectroscopic measurements of asteroids allow mitigation of differential color refraction effects on ground-based astrometry and orbit prediction accuracy

Spectroscopic measurements of asteroids allow mitigation of differential color refraction effects on ground-based astrometry and orbit prediction accuracy

Roman Geykhman, Kerri Cahoy

Roman Geykhman, Kerri Cahoy, "Spectroscopic measurements of asteroids allow mitigation of differential color refraction effects on ground-based astrometry and orbit prediction accuracy," Proc. SPIE 10702, Ground-based and Airborne Instrumentation for Astronomy VII, 107024U (6 July 2018); doi: 10.1117/12.2312230

SPIE.

Event: SPIE Astronomical Telescopes + Instrumentation, 2018, Austin, Texas, United States

Spectroscopic measurements of asteroids allow mitigation of differential color refraction effects on ground-based astrometry and orbit prediction accuracy

Roman Geykhman[1] and Kerri Cahoy[1]

[1]Department of Aeronautics and Astronautics, Massachusetts Institute of Technology, Cambridge, MA

ABSTRACT

Data collected with ground-based telescopes accounts for the overwhelming majority of astrometric observations of main-belt and near-Earth asteroids. Earth's atmosphere subjects these measurements to random error from seeing and to systematic bias from differential color refraction (DCR). The DCR bias when observing solar-illuminated targets with nonuniform spectral reflectances and using non-solar-analog stars as fiducials can be several tens of milliarcseconds, even at low airmass. The direction of DCR bias is aligned with local vertical at the observing telescope and its varying orientation in inertial space masks its signature in aggregate error analysis performed in inertial coordinates. Until recently, DCR effects of tens of milliarcseconds were dominated by the hundreds of milliarcseconds of systematic bias present in astrometric star catalogs. Improvements in the accuracy of catalogs beginning in 2015 with the 30 milliarcsecond URAT1 catalog, the 2017 publication of the 25 milliarcsecond UCAC5 catalog, and the forthcoming sub-milliarcsecond GAIA catalog have lowered the error floor on achievable accuracy to the point where DCR is now the dominant systematic bias in data taken from the ground. DCR bias depends on the spectral quantum efficiency of the observing instrument, the spectral reflectance of the target, and the spectral types of the fiducial stars. To realize the benefit of star catalogs accurate below the 30 milliarcsecond level, spectroscopic measurements of asteroids and fiducial stars are necessary to correct for DCR bias.

We analyze archival observations of asteroids with known spectral types and present new findings with our own high-volume observations of GPS and GLONASS satellites and the asteroids 4179 Toutatis and 3122 Florence reduced using the URAT1 and UCAC5 catalogs to show that DCR, rather than catalog bias, is now unambiguously the dominant source of systematic error in ground-based astrometry. Our observations of 3122 Florence with the r' and i' passbands exhibit vertical residuals more than 100 milliarcseconds beyond what we predict using published reflectance spectra. We attribute the discrepancy between prediction and measurement to the high sensitivity of predicted DCR bias to the slope of the asteroid's spectral reflectance within the r' and i' passbands and caution against relying on narrow passbands alone to mitigate DCR bias. We derive requirements for measurements of instrument spectral quantum efficiency and asteroid spectral reflectance necessary to compensate for DCR to a level commensurate with the accuracy of modern catalogs. The instrument passband must be well-sampled, and while a spectral resolution of 75 nm is sufficient on average when using an unfiltered silicon detector, a resolution of 10 nm is required to ensure worst-case astrometric accuracy of 25 milliarcseconds when observing asteroids with Sloan passbands down to zenith distances of 75 degrees.

Systematic biases of tens of milliarcseconds correspond to kilometers of instantaneous cross-range error when observing asteroids. For certain geometries, that error builds with more data rather than averaging out. We examine all likely Earth-impact scenarios and find that when an asteroid approaches from inside 1 AU and forces ground-based observations to occur at large zenith distances, lack of DCR compensation results in impact point predictions that are biased significantly away from their true locations. We present hypothetical NEO discovery scenarios where at fewer than four months before impact, the bias in impact point estimates derived from available ground-based data is many hundreds of kilometers beyond the five-sigma formal uncertainty of the estimate.

1. INTRODUCTION

1.1 Background

Until the mid-2010s, the astrometric accuracy of ground-based optical observations has been limited by the accuracy of the star catalogs used to reduce the observations. Advances made over the first half of this decade in the accuracy of star

Ground-based and Airborne Instrumentation for Astronomy VII, edited by Christopher J. Evans, Luc Simard, Hideki Takami,
Proc. of SPIE Vol. 10702, 107024U · © 2018 SPIE · CCC code: 0277-786X/18/$18 · doi: 10.1117/12.2312230

catalogs compiled from observations collected with ground-based telescopes have lowered this accuracy limit to below 30 mas and the forthcoming Gaia catalog[1] is expected to lower it to below 1 mas. These reductions in the systematic error on observations imposed by uncertainty in the locations of fiducial stars leave atmospheric effects as the dominant source of systematic error in ground-based astrometry.

Earth's atmosphere is a dispersive medium, meaning astrometric reductions on targets observed from the ground are subject to a systematic bias from differential color refraction (DCR). This bias depends on the targets' spectral reflectance, the spectral quantum efficiency of the observing instrument, and the spectra of the fiducial stars used for the solution. Systematic errors in astrometry propagate into systematic errors in orbit predictions. This is especially true for asteroids, which are almost exclusively observed with ground-based telescopes.[2] Further, telescopes employing silicon sensors optimized for detection sensitivity operate with passbands that are a wide fraction of the 300–1100 nm sensitive band of silicon[3] and are subject to DCR more than sensors using narrow passbands. Taken together with advancements in star catalog accuracy, the state of the art has reached a point where the accuracy of the orbit solution for any given asteroid is dependent on the accuracy of that individual asteroid's spectroscopic characterization. We analyze the interplay between spectroscopic characterization and orbit prediction accuracy for hazardous asteroids and derive resolution requirements for spectroscopic surveys of asteroids to achieve astrometric accuracy on par with that of presently-available star catalogs.

This paper is organized as follows. The remainder of this Section reviews the phenomenon of DCR bias, develops predictions for DCR bias of stars and of asteroids using published asteroid spectroscopic surveys, and reviews the state of the art for astrometric accuracy from ground-based telescopes. Section 2 presents empirical evidence that DCR bias is the error floor in ground-based astrometry by analyzing observations of GPS and GLONASS satellites, archived observations of asteroids with known spectral types, and targeted high-volume observations of the asteroids 4179 Toutatis and 3122 Florence collected at MIT and MIT Lincoln Laboratory (MIT/LL) facilities. Section 3 derives the resolution requirement for a spectrographic measurement campaign necessary to compensate for DCR bias to a level commensurate with star catalog accuracy and Section 4 provides further motivation for spectroscopic characterization by examining worst-case effects of uncompensated DCR bias on predictions of impact points of hazardous asteroids. Section 5 concludes with a summary of results and recommendations.

1.2 Differential Color Refraction

1.2.1 Phenomenology

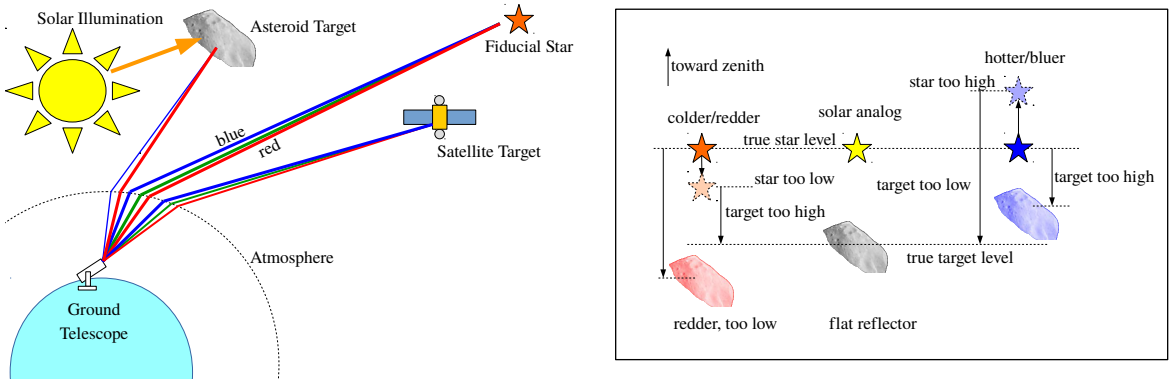

(a) DCR in cross-section (b) DCR in plate

Figure 1: Schematic of differential color refraction (DCR).

A schematic of DCR is shown in Figure 1. Shorter wavelengths bend more than longer wavelengths and thus all broadband point sources originating from space appear from the ground not as point-like PSFs but as compact vertically-oriented streak-like spectra with blue on top and red on the bottom. This applies to both targets and fiducial stars. The effect on the astrometric observation is reversed for targets and for stars. Red targets registered against solar-analog stars appear to be systematically lower, but solar-analog targets registered against red stars appear to be higher than they would be if the fiducial star's spectrum matched the targets'.

Quantitative descriptions of DCR began to be published in the 1980s. Filipenko computed the energy distribution of the streak-like PSF as imaged on the ground for the purpose of mapping the wavelength dependence of the capture efficiency of a spectrograph slit not aligned with the local vertical[4] and Stone described the effect of DCR on astrometry for stars in the compilation of star catalogs.[5] With detectors commonly used for astrometry in the mid-1980s, DCR was predicted to introduce no more than about 50 mas of bias into the angle between solar-analogs and O and M type stars. This error level was of little practical importance at the time given the inaccuracies of then-available fiducial star catalogs, but the combination of improvements in catalog accuracy to below 30 mas and the wide-spread use of high sensitivity broad-band silicon CCD imagers in asteroid search motivates a re-examination of the significance of DCR.

1.2.2 DCR Calculation

The procedure to compute DCR bias in relative astrometry described here follows Stone and Filipenko. At a zenith distance z, assume that the target has a detectable photoelectron spectral flux density defined by $\phi(\lambda, z)$, and that the total refraction as a function of wavelength at that zenith distance can be computed as

$$y = \Delta z(\lambda, z) = f(\lambda, T, P, RH, z) \tag{1}$$

where the symbol y is the spatial vertical coordinate on the focal plane corresponding to wavelength λ, and the local meteorological conditions are defined by temperature T, pressure P, and humidity RH. DCR transforms the spectral flux density into an angular flux density which appears as a spatial flux density on the telescope's focal plane. This density is given by

$$\psi(y) = \phi(f^{-1}(\lambda, T, P, RH, z), z) \tag{2}$$

We take the vertical centroid δz_0 of that flux density to compute the total shift with respect to some arbitrary zero-point of the definition of $f(\cdot)$ at that zenith distance via

$$\delta z_0 = \frac{\int_\lambda \psi(y) y}{\int_\lambda \psi(y)} \tag{3}$$

For relative astrometry, the quantity of interest is the shift with respect to either a star spectrum or the solar spectrum, meaning the DCR bias δz is defined by

$$\delta z = \frac{\int_\lambda \psi_{\text{target}}(y) y}{\int_\lambda \psi_{\text{target}}(y)} - \frac{\int_\lambda \psi_{\text{star}}(y) y}{\int_\lambda \psi_{\text{star}}(y)} \tag{4}$$

The total detectable photoelectron flux for both target and star is the product of vacuum spectrum, atmospheric spectral transmittance $t(\lambda, z)$, and the total instrument spectral quantum efficiency $\eta(\lambda)$. The vacuum spectrum of asteroids and satellites is the product of the vacuum solar flux density $\Phi_{\text{sun}}(\lambda)$ illuminating the target with the target spectral reflectance $r(\lambda)$.

Note that both the refraction angle and the wavelength-dependent target flux are a function zenith distance. The wavelength dependence of the refraction angle may be computed rigorously via the Auer-Standish algorithm[6] or approximately as $\Delta z \propto \sec z$ with standard wavelength-dependence relations for the refractive index of air. The fact that the calculation is for a relative offset lowers the sensitivity of the result to the accuracy of the amount of total bending. Atmospheric transmittance profiles are computed using MODTRAN[7] with the standard surface pressure, temperature, humidity, and meteorological visibility specified as inputs.

The spectral sensitivity of a telescope is the product of the spectral quantum efficiency of the detector and spectral efficiency of the optics. In this work we consider a typical arrangement of two aluminum-coated mirrors, a quartz corrector lens, and quartz dewar window. The spectral reflectance of mirrors are estimated from handbook optical properties of aluminum,[8] and quartz windows and lenses are assumed to have flat transmittance across the entire silicon band.[9]

An example result of a calculation for the vacuum-to-detection sensitivity at two different elevation angles for a sensor employing a deep depletion detector[10] near sea level is given in Figure 2. The differential refraction between the red and blue ends of the effective detected signal is on the order of several hundred milliarcseconds even at low zenith distance and can reach several arcseconds at an elevation of 30°. Refraction (and thus DCR) is greater at shorter wavelengths and at lower elevations. The interplay between simultaneously increasing refraction and decreasing detection sensitivity in the blue end of the silicon band at lower elevations is complex and will be explored further in the next two Sections.

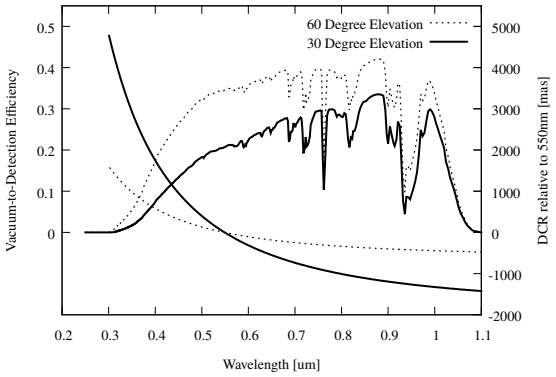

Figure 2: Total vacuum-to-detection efficiency and DCR versus wavelength near sea level

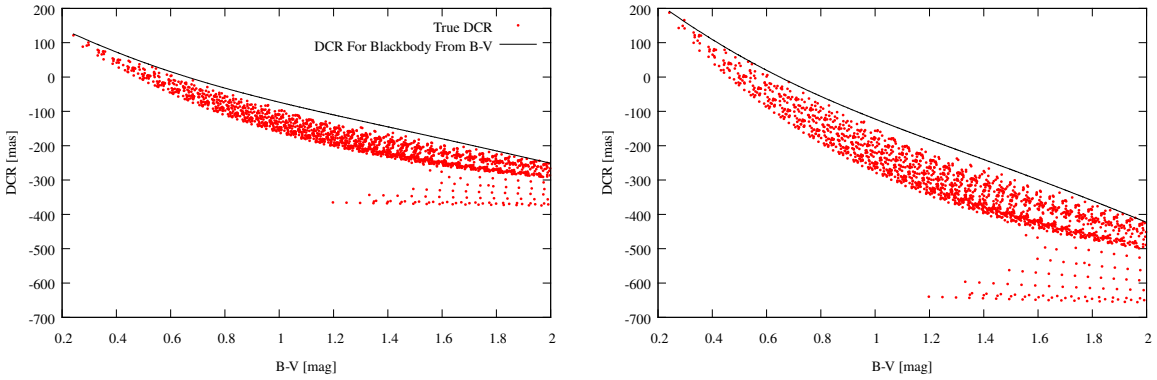

(a) 45° elevation (b) 25° elevation

Figure 3: DCR of reddened stellar spectra vs DCR of blackbody spectra inferred from $B-V$ with bare silicon detector at sea level. Pickles Atlas spectra are subjected to interstellar reddening between 0.01 and 4.0 kpc. Synthetic photometry in Johnson B and V bands is computed and a color-temperature relation[13] is used to synthesize an (unreddened) blackbody spectrum. The DCR for the blackbody spectrum and all DCRs for true spectra are plotted assuming sea-level atmosphere and a standard silicon quantum efficiency. The blackbody approximation is best for near sun-like stars at short distances, and this is indicated by the small number of points tangent to the blackbody baseline near $B-V \approx 0.6$.

1.2.3 DCR of Stars

Most stars are not Sun-like and their spectra are subject to interstellar reddening. The ability to predict the DCR of stars is limited by the ability to infer the combined effects of spectral type and amount of extinction from the multi-color photometry available for each fiducial star in the compiled catalog. Stone's analysis of the narrow passbands used for high-precision astrometry shows that the distinction between interstellar reddening and spectral type is not significant and it is possible to infer DCR directly from $B-V$. This does not extend to the wider pass-bands of modern silicon detectors used for asteroid search.

Using standard relations between visible band extinction $A(V)$ and per-wavelength extinction[11] and a representative collection of stellar spectra such as the Pickles Atlas,[12] one may simultaneously vary spectral type and interstellar reddening, compute synthetic photometry in Johnson B and V bands, and compare the DCR for the actual spectrum of the star with the DCR for an unreddened spectrum inferred from the $B-V$. An example calculation of the discrepancy between reddened spectra and blackbody spectra is shown in Figure 3 where it is clear that a calculation based only on $B-V$ correctly estimates DCR vs color slope but systematically underestimates the absolute amount of stellar DCR with respect to a solar spectrum.

A better estimate of DCR bias combining the effects of both reddening and spectral type can be made from multi-color photometry spanning both the visible and near infrared bands. Section 2.3 provides empirical evaluation of the quality of stellar DCR correction using both two-color blackbody estimation and multi-color reddening-aware estimation.

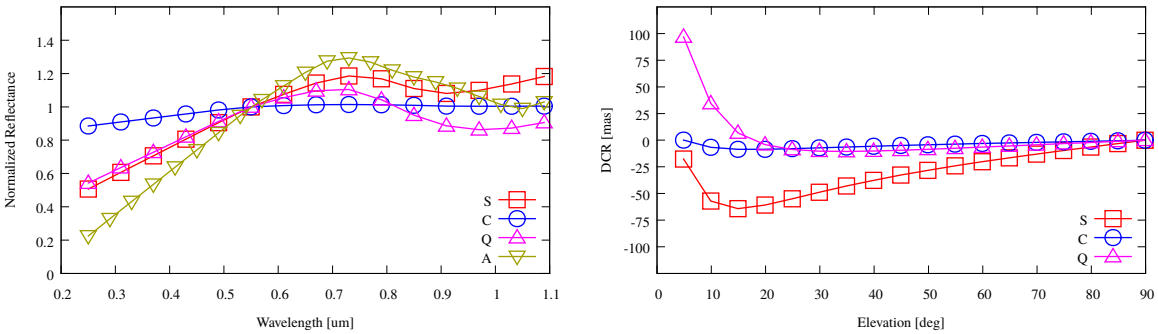

(a) Reflectance spectra of selected SMASS classes

(b) Bias vs elevation at 1.6km altitude

Figure 4: Asteroid spectral reflectance and predicted DCR bias. While the A-type spectrum has the greatest slope, it is uncommon. The C-type and S-type asteroids are the most numerous representatives of near-flat spectral slope and large spectral slope, respectively. Many asteroids' spectra fall between S-type and Q-type. DCR is computed using nominal atmospheric conditions for a deep depletion silicon detector at Socorro, NM.

1.2.4 DCR of Asteroids

Asteroids' spectral reflectances have been well-studied beginning with multi-color photometric campaigns conducted in the 1970s[14] up through the SMASS surveys[15,16] in the 2000s. However, the number of asteroids with spectral measurements is a small fraction of numbered asteroids. Further, the majority of SMASS observations did not measure bluer than 450 nm. Because silicon has sensitivity below that wavelength and the atmosphere has appreciable throughput below that wavelength at high altitudes and low zenith distances, there is a gap in the ability to predict DCR for many spectroscopically-characterized asteroids.

For this analysis, we consider the S and C type asteroids in the Bus-Demeo classification system.[17] These represent the most common type of the extreme cases of near-flat spectral reflectance and most sloped spectral reflectance. As the majority of reflectance spectra for these asteroids are only measured down to 450 nm, it is necessary to extrapolate to cover the full silicon band. Tholen[18] and Chapman's[14] early multi-band photometric surveys of the asteroid belt included coverage down to 300 nm and examination of the that data for C-type and S-type asteroids indicates that linear extrapolation down from 450 nm to 300 nm is a valid operation. The resulting reflectance spectra used in this analysis and computed DCR bias are shown in Figure 4.

An important consideration is the variability of DCR bias with local atmospheric conditions. Setting aside the question of how to compensate for stellar DCR, we consider the difference between the DCR of S-type and C-type asteroids. This quantity was computed over a wide variety of atmospheric conditions and altitudes and is shown in Figure 5. While the DCR difference is only weakly sensitive to surface temperature, pressure, and relative humidity, it is sensitive to site altitude and the spectral quantum efficiency of the detector and is highly sensitive to meteorological visibility. The sensitivity to meteorological visibility is greatest below 30 degrees elevation. The DCR bias and its sensitivity to meteorological conditions is higher at higher altitude sites than at lower altitude sites because of the decreased attenuation at higher altitude of the blue end of the target's spectrum where refraction is greatest outweighs the reduction in refraction and DCR at higher altitude.

1.3 State of the Art Observation Accuracy

1.3.1 Star Catalog Accuracy

While high-accuracy fiducial star catalogs on bright stars have been available for many decades, in order to be useful for astrometric reduction on asteroids, catalogs must have a sufficient density of stars within a small-enough field of view and of comparable signal strength to the target being observed in order to stay within the geometric and dynamic range limits of the observing instrument. Densities on the order of one hundred stars per square degree are required for practical astrometry with telescope fields of view on the order of half a degree. Until recently, the accuracy of star catalogs with a sufficient density of faint stars has been limited.

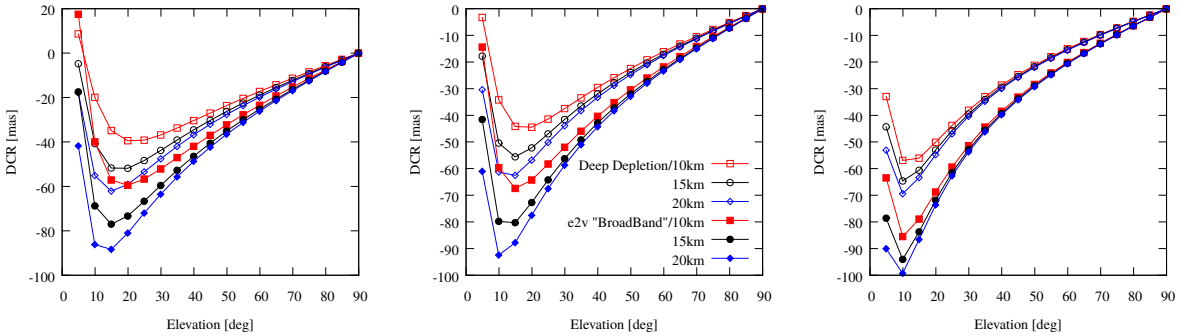

(a) Sea level (b) 1.6 km altitude (c) 3.0 km altitude

Figure 5: Variability of difference in S-type and C-type asteroid DCR bias with meteorological conditions and detector type. Deep depletion and ordinary silicon detector quantum efficiencies taken from e2v Corporation datasheets.[10] The three altitudes represent much of the range of altitudes of stations contributing observations into the Minor Planet Center and the three meteorological visibility conditions are representative of real-world extremes. There is little sensitivity to surface temperature, pressure, and humidity and traces examining variation in those parameters are not shown.

The first modern deep-sky astrometric catalog was the Palomar All-Sky Survey, conducted in the 1950s. The Schmidt plates from that survey and its Southern Hemisphere counterpart were digitized in the early 1990s as the USNO-A and USNO-B series of star catalogs, yielding a catalog complete to V=20 but only accurate to 0.2 arcsec.[19] The first space-based astrometric catalog, from the European Space Agency's Hipparcos mission, became available in the late 1990s, and while accurate to single-digit milliarcseconds, was only complete to V=12, or a density of fewer than tens of stars per square degree.[20] Ground-based observations conducted by the US Naval Observatory with CCD astrographs in the early 2000s yielded the UCAC series of star catalogs, which became available[21] in 2009 with a completeness to V=16 which is sufficient for practical use in astrometry with relatively narrow fields. Final reductions of this dataset were completed in 2013 resulting in the UCAC4 catalog with a claimed accuracy of under 40 mas.[22] A second data collection campaign in the early 2010s with improved instrumentation yielded the URAT1 catalog, comprising only the Northern Hemisphere sky, with more accurate proper motions, a slightly fainter cut-off, and a claimed accuracy of 30 mas.[23]

Throughout the 2010s, the European Space Agency's Gaia mission has been operating as a follow-on to the Hipparcos satellite. This mission promises to yield parallaxes as well as proper motions and aims for sub milliarcsecond accuracy to V=19. The final data release with the full astrometric solution is expected in the 2020s, but the first data release containing positions, but not proper motions for faint stars, appeared in late 2016.[24] When the final data release is made, the density of high-precision fiducial stars will approach that of the USNO-B catalog. In the interim, re-reduction of the UCAC dataset using both Hipparcos and Gaia DR1 data has yielded the UCAC5 catalog, containing the same all-sky coverage to approximately V=16 with astrometric accuracy improved to the sub-30 mas level.[25] We note that although the recent publication of Gaia Data Release 2 provides an all-sky sub-mas star catalog, the majority of data collected up through the late 2010s is limited by the UCAC and URAT catalogs' accuracy.

1.3.2 Ground-Based Observation Accuracy

As DCR is not new, many astronomical observing programs take steps to mitigate it by observing through narrow bands and at low zenith distances.[26] While this enables absolute astrometric accuracy on the order of 20 mas when employing accurate catalogs, as was achieved in the Gaia Ground-Based Optical Tracking campaign,[27] it comes at the cost of detection sensitivity and observing opportunities. This results in a reduction in data volume, leading to higher overall uncertainty in an orbit estimate. We focus here on the state of the art in accuracy achieved by sensors operating with bare silicon detectors, whose improved detection sensitivity over narrow-band sensors makes them more suitable for asteroid search and which account for a large majority of astrometric observations of all asteroids.

The accuracy of astrometric observations has kept pace with advancements in star catalog accuracy. Carpino's analysis[28] shows that the precision of individual measurements is limited by an error floor of about 250 mas. That error floor is imposed by the spatial variability in star catalog errors and random error from atmospheric turbulence as integrated over exposures suitable for single-frame detection of typical asteroids. Work with high frame-rate detectors and image stacking

techniques by Shao[29] and Zhai[30] has made it more practical to move past the turbulence-imposed error floor and to realize the benefit of the improving accuracy of modern star catalogs.

This point bears further elaboration. The 250 mas error floor is a random error that is subject to attenuation by incorporation of more data over the observing arc and with image stacking techniques. The attenuation of the time-varying random error exposes underlying systematic errors. Work in identifying the magnitude of those systematic errors has focused on looking at the the correlation coefficients of nearby observation residuals of asteroids with long observing arcs and/or multiple radar apparitions. Carpino found that the day-to-day correlation coefficient reached a level of approximately 0.015 by the late 1990s. This implies the presence of a low-frequency signal with a strength on the order of $250 \times \sqrt{0.015} \approx 30$ mas. At the time of Carpino's analysis, most observations were made with the older star catalogs and that underlying signal was attributed to fixed-pattern catalog bias. Farnocchia's re-analysis with after-the-fact star catalog corrections[31] shows marginal reductions in observation residuals, but that a portion of that systematic error signal remains. This paper makes the case that this residual systematic error is consistent with DCR bias and the state of the art in astrometric observations has reached the point where DCR sets the error floor.

2. EXISTENCE OF DCR IN REAL DATA

2.1 DCR Bias in Observations of GPS and GLONASS Satellites

To demonstrate that the dominant systematic error in astrometry with modern star catalogs is atmosphere-induced, we analyze observations of GPS and GLONASS satellites collected at the MIT Lincoln Laboratory Firepond Optical Facility in Westford, MA. The Firepond facility has been in operation since 2010[32] and regularly observes GPS and GLONASS satellites as part of its calibration procedures. Raw image data from these observations dating back to 2012 was obtained and re-reduced using the URAT1 star catalog. The observations were compared against final satellite state estimates from the International GNSS Service, which are accurate to the 10 cm level.[33] This is smaller than the physical extent of the satellite. If the satellite's radius with respect to its antenna phase center is assumed to be on the order of 2 meters, the worst-case error budget for the apparent location of the optical centroid with respect to the truth ephemeris is approximately 20 mas. We thus expect this measurement to be accurate to at worst the sum of this offset with the catalog error and on average to be dominated by the catalog error.

The observation residuals are resolved into station horizon-aligned coordinates rather than being left in inertial coordinates in order to highlight the presence or absence of atmospheric effects. By symmetry, atmosphere-induced biases would have no signature in the horizontal component of the residuals. Vertically-aligned systematic errors would be expected to average to non-zero values and in aggregate to have more spread than horizontal residuals.

The residuals of approximately 165,000 distinct observations are plotted in Figure 6. On average, the mean horizontal residual is near zero in all elevation bins. The majority of the outlier peaks for both GPS and GLONASS targets are consistent with a catalog bias of no more than the 30 mas claim of the URAT1 catalog summed with the worst-case effect of the physical extent of the satellite. While some outliers in the horizontal coordinate do exist in some elevation bins, the presence of consistent near zero-mean horizontal errors for much of the span of elevation indicates good overall astrometric data quality.

Confidence in the astrometric reductions derived from that near-zero mean horizontal error allows the claim to be made that the behavior of the vertical residual in the same region unambiguously indicates atmosphere-induced bias. Before attributing all the residual error to DCR, a word of caution is warranted about observing near-Earth targets. Parallax is not negligible at GPS altitudes, and although parallax is weakly sensitive to variations in local atmospheric conditions, it is monotonic with absolute refraction and thus any correction for parallax applied to the data is sensitive to an absolute error in the computation of total refraction. The error in models used to estimate total refraction at elevations below 30° can be several tens of percent.[34]

Nevertheless, parallax is smoothly-varying with elevation for targets at a near-constant orbital altitude and structure in the shape of vertical residuals with elevation after parallax has been removed can serve as evidence of DCR. The residual structure in our data is consistent with stabilized spacecraft with sun-tracking solar panels whose apparent aspect to the observing site (and spectral signature) varies systematically with elevation angle. GPS and GLONASS targets are in repeating ground-track orbits and one would expect fairly strong coupling between phase and elevation angles from a

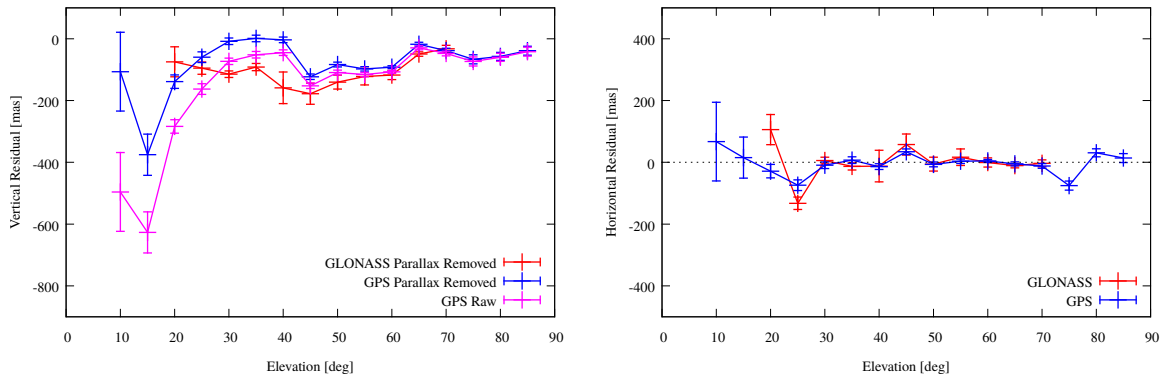

(a) Vertical residuals

(b) Horizontal residuals

Figure 6: Residuals of Firepond observations of GPS and GLONASS satellites reduced with URAT1. Mean and $\pm 3\sigma$ of mean residuals in evenly-spaced elevation bins. N=130,000 observations of GPS satellites and 35,000 observations of GLONASS satellites. Star DCR corrections are not applied.

single ground site. The separation in traces between the vertical residuals of the GPS and GLONASS satellites is indicative of spacecraft in different orbits presenting different aspect angles and of the difference in surface materials of two different spacecraft constellations. Thus, despite the fact that it is not completely possible to separate DCR bias from parallax in this dataset without spectroscopic observations of satellite targets, the confinement of systematic error to the vertical coordinate and the structure in the parallax-corrected residuals unambiguously indicate that DCR exists in real data and dominates the systematic error floor in astrometry.

2.2 DCR Bias in Archived Minor Planet Observations of Asteroids

To bypass the ambiguity introduced by parallax bias for near-Earth targets and to take advantage of targets with well-defined reflectance spectra, we examine archived observations of asteroids with known spectral types. The S-type asteroids make up the largest group of asteroids with the highest spectral reflectance slope in the silicon band and the C-type asteroids make up the largest group with a nearly flat spectral scope over that band. We examine archived observations of asteroids belonging to those two classes and to bypass uncertainty about the DCR of fiducial stars, we consider the difference between vertical residuals of S-type and C-type asteroids.

Figure 7 shows the horizontal and vertical residuals for the two asteroid classes from all contributing stations archived in the Minor Planet Center database, and just those from the LINEAR program. There is, indeed, a separation between the two types in the vertical coordinate that does not appear to exist to the same level of statistical significance in the horizontal coordinate. However, the common-mode structure in both the vertical and horizontal residuals makes it difficult to attribute all of the systematic error to atmospheric biases.

The limitation that causes this ambiguity is the accuracy of the star catalogs used to make the data reduction. A large fraction of the Minor Planet Center archive consists of observations made by the LINEAR program. Considering only observations from that sensor, one sees that there is quite a bit of common mode structure in both horizontal and vertical residuals. The bump in the vertical residual at an elevation of about 40 degrees corresponds to a declination of about -20 degrees. The LINEAR system came online in the mid 1990s and used the USNO astrometric catalogs available at that time, which were compiled from scans of Schmidt plates of separate northern and southern hemisphere surveys. The seam between the two surveys occurred around that declination band, and the error in joining the two datasets propagated into the LINEAR data and dominates the systematic bias for the entire Minor Planet Center archive.

With the publication of the Farnocchia catalog corrections[31] to the USNO catalog, it became possible to remove this error from the LINEAR data and from other early observations. When that is done, the common mode in the horizontal coordinate of the residuals disappears, any spurious separation in the mean horizontal residuals for the two classes of asteroids disappears, and the common mode error in the vertical coordinate is greatly attenuated, while the separation in the vertical residuals remains. This difference between like-kind observations where the only distinction is the spectral

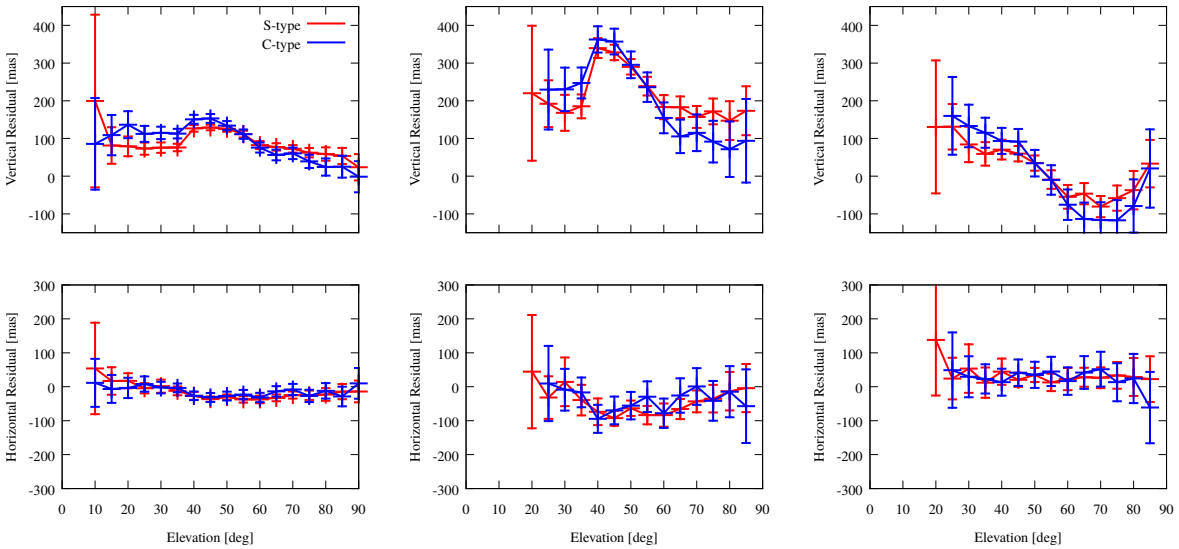

(a) All ground telescopes (b) LINEAR, no debiasing (c) LINEAR, debiased

Figure 7: Horizontal/vertical residuals of archived observations of S-type and C-type numbered asteroids. Mean $\pm 3\sigma$ of the mean residual versus elevation with respect to JPL best estimate ephemerides retrieved Nov 2017.[35] Observations retrieved from IAU Minor Planet Center[2] Jan 2017. Aggregate data from all stations spans calendar year 2000 to 2016. The LINEAR system observations span the calendar years 2000-2012 when the original LINEAR program was shut down and replaced by the Space Surveillance Telescope. The total number of LINEAR observations consists of approximately 50,000 observations of C-type asteroids and 120,000 observations of S-type asteroids.

type of the object observed supports the hypothesis that DCR dominates the systematic error in observations of asteroids made with bare CCDs.

2.3 High Volume Observations of Individual Asteroids

The corrected residuals in Figure 7(c) are still less than completely satisfying in terms of providing unambiguous proof that DCR bias dominates the error in ground-based astrometry of asteroids using modern star catalogs. While all the systematic bias is confined to the vertical coordinate, the shape of the vertical residual does not match the prediction in Figure 4(b) and the difference between the two types' vertical residuals changes sign at 55° elevation contrary to the predictions in Figure 5. The relatively small number of observations within each elevation bin, coupled with the limited number of observations on any individual asteroid makes it difficult to say definitively say whether the discrepancy is caused by any of

1. Natural variability of spectral slopes and absorption band shapes among individual asteroids within the same class
2. Variability in the spectral types of the stars individually used for the data reduction of each observation
3. Variability in meteorological visibility at the time of each individual observation

While it is theoretically possible address the first concern by making predictions for the vertical residuals of individual asteroids using their individual reflectance spectra measurements, the small number of observations of each individual asteroid limits the utility of that approach. The latter two areas of ambiguity are not addressable using after-the-fact catalog corrections. For this reason, we continue this line of inquiry with targeted data collections on individual asteroids that we reduce using modern star catalogs.

On December 13, 2012, the Firepond facility observed the flyby of the S-type asteroid 4179 Toutatis as a target of opportunity for 45 minutes. The asteroid was sufficiently close and bright to enable fast framing, and approximately 2400 distinct astrometric observations were collected. The raw data from this pass was obtained and re-reduced using the URAT1 star catalog, and compared against the the JPL ephemeris for 4179 Toutatis, which had by that time incorporated a large number of optical observations from after the 2012 apparition and radar observations from the 2016 apparition. The scatter of the distribution of residuals resolved in station horizontal and vertical coordinates is shown in Figure 8, and it is indeed the

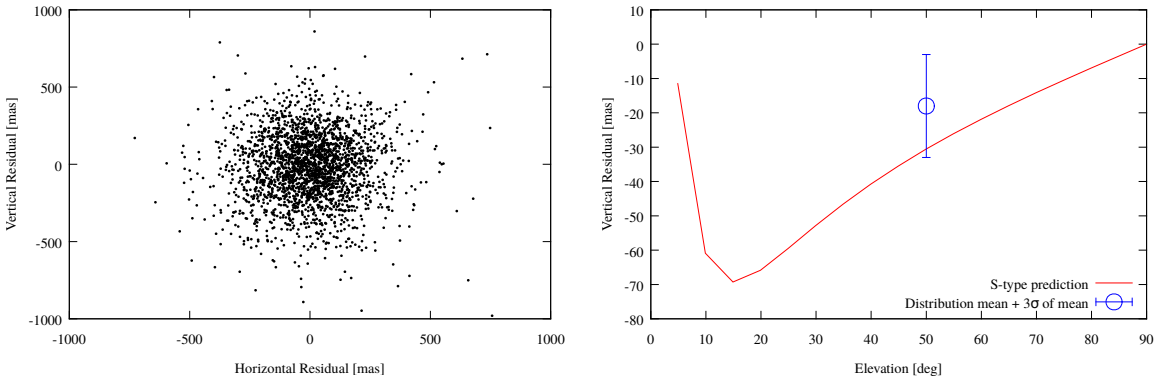

(a) Residuals scatter (b) Vertical distribution and prediction

Figure 8: Scatter of residuals of observations of 4179 Toutatis reduced with URAT1 and resolved in horizontal/vertical coordinates, along with vertical residual distribution overlayed on predictions for an S-type asteroid observed from Westford, MA. The mean horizontal residual is -0.5 mas and the mean vertical residual is -18.6 mas.

case that the horizontal error is zero-mean while the mean vertical error is nonzero to a 3σ confidence and is consistent with predictions for an S-type asteroid.

The experience with the 2012 flyby of Toutatis motivated a dedicated observing campaign to target the 2017 flyby of 3122 Florence. On the nights of August 31 and September 1, 2017, MIT/LL sensors at the Experimental Test Site (ETS) in Socorro, NM, the Firepond facility, and the MIT Wallace Astrophysical Observatory (WAO) in Westford, MA observed the flyby. The MIT/LL sensors observed with bare silicon detectors and the Wallace site observed through Sloan r' and i' passbands. The nearest approach distance was about 7 million kilometers and the object peaked at a brightness of about V=8, enabling observations at 8Hz from the bare CCD sensors and 0.5 Hz from the filtered sensors. Target motion was about 0.5 arcsec / sec with respect to the star background and a wide diversity of elevation angles were covered by the pass. All stations observed GPS and GLONASS satellites in order to calibrate shutter timing accuracy against the horizontal component of observation residuals of those satellites.

Overall, approximately a 250,000 distinct observations were generated across the three sites, with the majority coming from bare CCD observations at Firepond and ETS. This is several orders of magnitude more data than is available for any long-arc numbered asteroid, and because it comes from the same sensors and observes the same target with the same reflectance spectrum, the low formal error on the residuals allows more concrete conclusions to be drawn about DCR than from analyzing low-volume observations in the MPC archive or even reprocessing the imagery used to generate that low number of observations of heterogeneous targets.

Observation residuals for all stations were first calculated against the JPL reference orbit and found to be significantly off from the estimate in the horizontal coordinate (Figure 9(a)). The same error was not present in calibration measurements of GPS and GLONASS satellites taken at the Firepond and ETS facilities during the observing session and the bias was attributed to a real error in the JPL orbit estimate. The magnitude of the error in the horizontal coordinate indicated a cross-range shift of a few kilometers. This was consistent with the published uncertainty of the right ascension of the ascending node of the orbit.

To obtain a better reference trajectory, a refined orbit fit was computed using published radar data from the close approach and optical observations contributed to the Minor Planet Center from other sensors. The force model used to compute the refined orbit was consistent with published details of the JPL force model[36] and verified against the JPL Horizons system. Only azimuth measurements were incorporated in order to free the result of DCR bias. Data was restricted to observations contributed during the period between April and October 2017 for which Farnocchia debias corrections were available. The relative weight was spread evenly between sensors tasked for this high-volume collection and the rest of the contributors to the Minor Planet Center. The resulting horizontal residuals are more in line with expectations and are shown in Figure 9(b).

Analysis of the higher-volume data from the bare-silicon sensor at the Firepond facility enables a low-errorbar evaluation

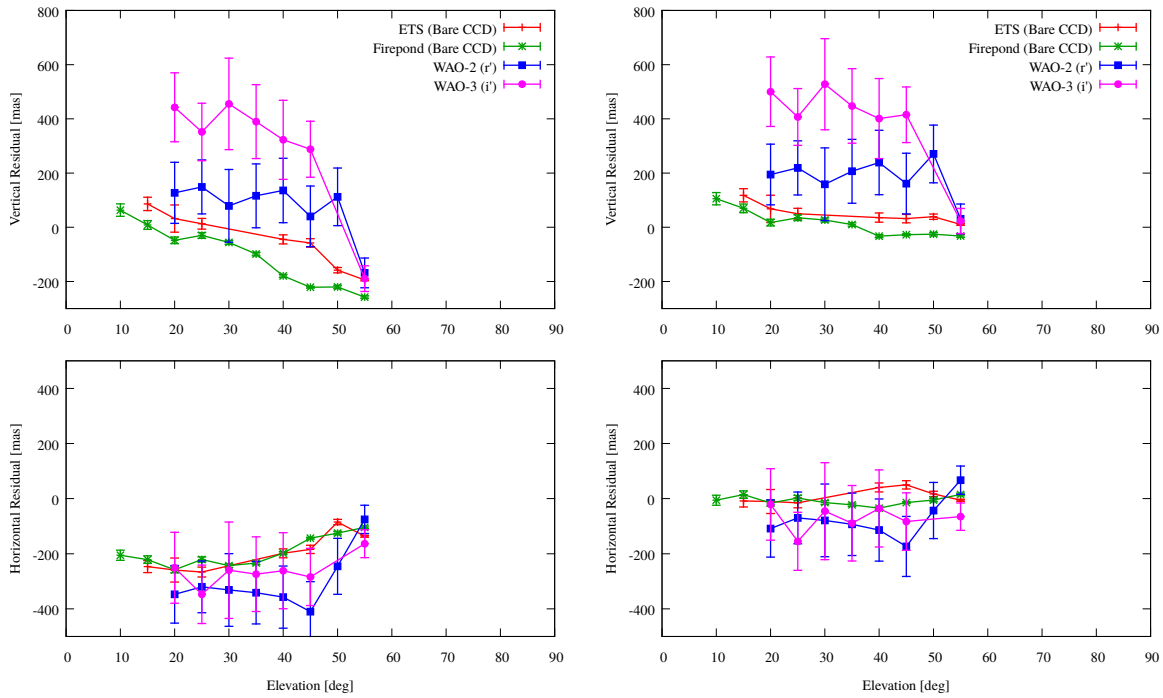

(a) Residuals vs JPL ephemeris

(b) Residuals vs azimuth-only refit

Figure 9: Mean $\pm 3\sigma$ of residuals vs elevation of 3122 Florence. JPL ephemeris retrieved 2017-11-12.

of the quality of the DCR predictions made using published spectra of 3122 Florence and DCR of stars using reddening-aware versus reddening-unaware corrections discussed in Section 1.2.3. Residuals of observations computed with URAT1 and UCAC5, with and without stellar DCR correction applied are plotted in Figure 10. 3122 Florence is identified as both an S-type and Q-type asteroid and overplotted on the residuals are the predictions of DCR for a bare silicon detector using generic S and Q class spectra as well as two direct measurements of the reflectance spectrum of 3122 Florence.

None of the residual traces from either catalog with either stellar DCR correction track any of the predictions particularly well. The raw URAT1 residuals track the prediction using Binzel's directly measured spectrum best but are systematically biased above it by a near constant offset that is inconsistent with fiducial star DCR. The raw UCAC5 residuals are systematically lower than the URAT1 residuals, which may indicate a systematic difference in the ensemble of stars contained in the URAT1 catalog and the UCAC5 catalog. Correcting the UCAC5 residuals for stellar DCR using reddening aware techniques leads to a worse result than the raw data and indicates either a systematic bias in the multi-band photometry in UCAC5 or a redder-than-expected spectrum of 3122 Florence at the time of observation. The two measurements taken with Sloan filters agree with the refined trajectory estimate in the horizontal coordinate to a level commensurate with the uncertainty in the smaller number of statistics coming from those sensors, but disagree more than expected in the vertical coordinate.

Taken in whole, the Sloan filter data serves as caution against reliance on narrow passbands to mitigate DCR bias and the amount of statistically-significant deviation from predictions from the bare CCD data from the Firepond facility provides support for the assertions that spectroscopic measurement of an asteroid is necessary in concert with astrometric observations and that spectroscopic spot-check measurements of fiducial stars are also necessary to verify the assumptions used to correct for stellar DCR.

3. SPECTROSCOPIC RESOLUTION REQUIREMENTS

3.1 Motivation

The error budget for the measurement of 3122 Florence was driven by the defect of illumination. Florence is about 5 km diameter[35] which at 7×10^6 km gives $\approx$ 100 mas angular extent. The vertical residuals from the Wallace site collected

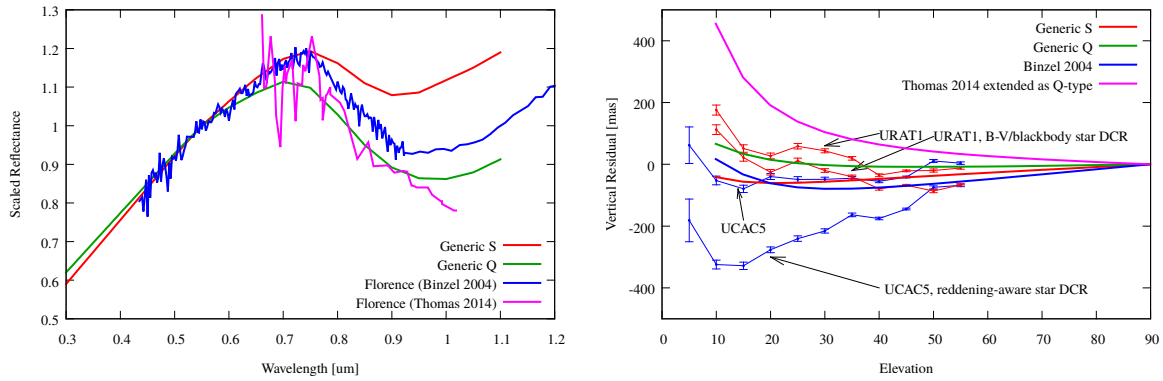

(a) Florence spectra (b) Firepond residuals and DCR predictions

Figure 10: Mean $\pm 3\sigma$ of mean vertical residuals vs elevation of Firepond bare silicon observations of 3122 Florence and predicted DCR biases from published spectra. Data reductions are made with both the URAT1 and UCAC5 star catalogs. Fiducial star DCR is computed differently for the two catalogs given the different multi-band photometry available in those catalogs.

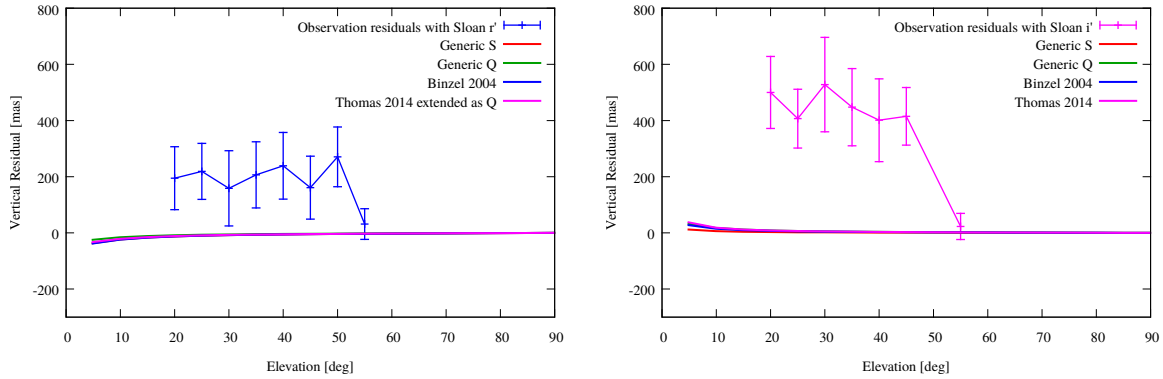

(a) WAO Pier 2 telescope (Sloan i') (b) WAO Pier 3 telescope (Sloan r')

Figure 11: Predictions of DCR bias of 3122 Florence observed through Sloan passbands[39] and mean $\pm 3\sigma$ of mean observation residuals vs elevation bin. The elevation bias seen in the observations from the Wallace site is not consistent with predictions by a statistically significant amount in excess of the measurement error budget.

with narrow filters exceed the worst-case bound for defect of illumination and greatly exceed the predicted DCR bias when observing with narrow bands (Figure 11).

This discrepancy can only be consistent with a difference between the modeled and actual target reflectance spectrum at the time of observation. The mismatch can be in the spectral slope across both of the passbands used for the observations or it can come from the presence of absorption features near the edges of the passbands. The difference in spectral slope can come from temporal variability in the shape the Band-I feature for the asteroid. Such variability has been observed as a function of observation phase angle[37] and can also be caused by variation in surface temperature for asteroids in eccentric orbits.[38] In either case, a spectroscopic measurement is necessary.

3.2 Approach

We derive the resolution requirement for that measurement by analyzing a hypothetical absorption feature in the continuum of the asteroid's reflectance spectrum. We assume a nominal reflectance spectrum for an asteroid and impose an absorption feature onto that spectrum. We then compute the true DCR bias of that perturbed spectrum to serve as the baseline and compute an estimated lower-resolution spectrum by averaging the perturbed spectrum with a boxcar filter defining the test resolution and subsampling. We estimate a DCR bias using the averaged and subsampled spectrum and compare with the baseline DCR. A resolution is considered sufficient if the worst-case DCR bias estimation error is under 25 mas at a zenith distance of 75 degrees.

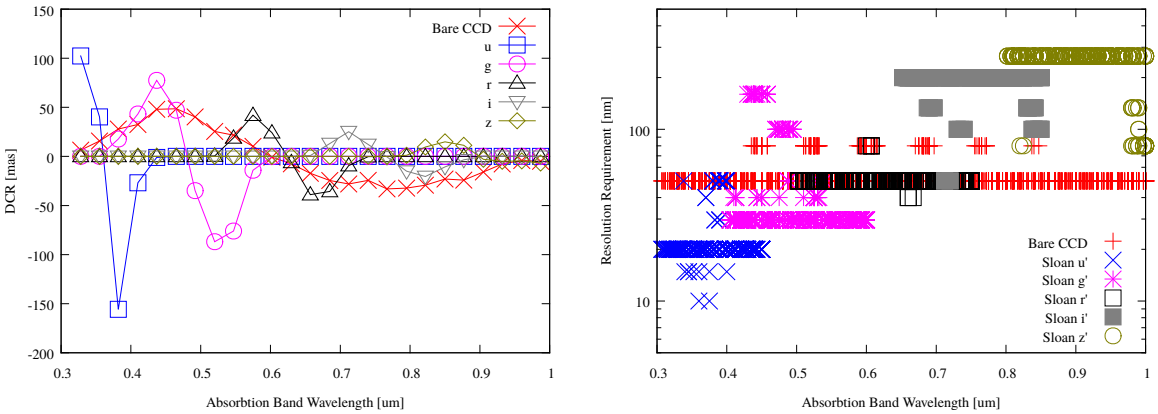

(a) DCR vs wavelength of absorption band

(b) Required spectral resolution

Figure 12: Resolution required for asteroid spectra with absorption bands. (a) The effect of a 55nm-wide, 75% absorption band on the DCR of an asteroid observed from the ground with respect to a reflectance spectrum without that band. (b) The spectral resolution required on the measurement of the target flux containing a 75 nm wide, 16% deep absorption band necessary to achieve a 25 mas accuracy on the DCR prediction as a function of the location of the absorption band and bands of smaller width but constant band area. The overall resolution requirement for any filter is the worst-case of an absorption feature within the filter passband exclusing individual outlier points corresponding to sensitivity to the particular shape of the band.

For unperturbed spectra, we consider the mean reflectance spectra for SMASS C, S, and Q asteroid classes, linearly extrapolated to 300nm. We scan a single absorption feature over the entire sensitive band of silicon to construct the perturbed spectra. The boxcar averaging and subsampling operation is performed using the spectrum weighted by atmospheric transmittance and instrument overall quantum efficiency. The calculation is made for the bare CCD and for individual Sloan[39] bands for sea level altitude, 1.6 km altitude representing the LINEAR system's location in New Mexico and 3.0 km altitude representing Haleakala, Hawaii. An example intermediate calculation showing the sensitivity of DCR bias to the location of the absorption band is shown in Figure 12(a) with an exaggerated 55nm wide 75% deep absorption band.

The absorption band used in this calculation was square with a depth of 16% and a width of 75 nm. The simulation showed little sensitivity to varying the width of the band while keeping the band area constant. An obvious question is whether these features actually occur in the reflectance spectra of real asteroids. In some C-type asteroids, small absorption bands in the continuum in the region between 700 and 900nm are up to 50nm wide and up to 5% deep.[40] Other common absorption features exist through much of the visible band redward of 500nm,[41] and for asteroids in eccentric orbits, temperature dependence and phase angle dependence may amplify them.[37,38] While it is unlikely that individual absorption bands as strong as that used in this calculation exist, the experience with narrow-band observations of 3122 Florence indicates that caution is warranted in assuming narrow passbands can mitigate DCR bias and support the claim that high-resolution measurements of the spectrum as detected on the ground are necessary.

3.3 Resolution Requirement

Figure 12(b) shows an example of the exhaustive simulations of the resolution requirement for the Westford, MA. The figure plots for each filter the necessary resolution over which the averaging and subsampling of the ground spectrum is sufficiently fine to enable DCR estimation to within a 25 mas accuracy down to a zenith distance of 75 degrees as a function of the location of the single absorption band. The calculation varies the width and depth of the absorption band while keeping the area constant at 75 nm $\times$16%. Analogous simulations were generated for the 1.6 km altitude of Socorro, NM and the 3.0 km altitude of Haleakala, HI assuming both deep depletion and ordinary cooled silicon quantum efficiency.

Unsurprisingly, because the sensitivity of DCR estimation for a given pass-band from a coarsely sampled spectrum is greatest near the edges of the passband, we see an inverted U shape on the resolution requirement for each filter. Further, because the refraction slope $d\Delta z/d\lambda$ is greater in the blue, the requirement is tighter for the u' and g' passbands than it is for the redder filters.

We quote the worst-case requirement for every filter over all three asteroid types observed at 15° elevation as the require-

ment for observing with that filter. The requirements are summarized in Table 1. As stated, there is little sensitivity of the resolution requirement to the shape of the absorption band so long as the depth-width product remains constant. An exception to that statement is the small number of simulation points corresponding to the u' and g' prime filter that lie below the overall resolution requirement shelf for those filters. We do not include those outlier points in our overall tabulation of requirements on the grounds that the square absorption band is only a calculation aid, not a physical phenomenon and a different band shape would lead to a slightly finer or coarser requirement.

Overall, the simulations indicate that a 20nm resolution is the bare minimum to observe in the u' band in order to achieve DCR compensation comparable to catalog accuracy of 25 mas down to a zenith distance of 75 degrees. Given the few outlier points mentioned in the previous paragraph, and the unexpectedly-large residuals of 3122 Florence observed with Sloan filters shown in Figure 11, it is appropriate to treat the results of this simulation with caution and to append a safety factor. We thus recommend a 10nm resolution when observing with bluer filters, and a 25-40 nm resolution when observing with redder filters or bare CCDs.

Table 1: Calculated resolution requirements to correct observations of asteroids to 25 mas

Site (Altitude)	Westford, MA (0.1 km)		Socorro, NM (1.6 km)		Hawaii (3.0 km)	
Pass Band	Regular Silicon	Deep Depletion	Regular	Deep	Regular	Deep
Bare CCD	50	50	50	50	50	80
u'	20	20	20	20	20	20
g'	30	30	30	30	40	40
r'	50	50	50	50	50	50
i'	133	200	20	200	200	200
z'	80	266	133	266	133	266

4. SIMULATIONS OF ASTEROID IMPACT SCENARIOS

To further motivate the necessity of spectroscopic characterization of asteroids, we examine the worst-case effect of DCR bias on the impact point predictions for hazardous asteroids. We assume that stellar DCR can be fully modeled and removed from the data, leaving only the target-dependent portion of the DCR unknown. As before, we assume that the unknown amount of DCR corresponds the difference between the DCR for S-type and C-type asteroids.

4.1 Impact Scenario Definition

The worst-case scenario for DCR bias is of an asteroid that is detected a short time before impact and for which the majority of astrometric observations come from ground-based optical sensors at high zenith distances. Such a set of scenarios is shown schematically in Figure 13(a). Assuming that the impact occurs on the outbound phase of the orbit ensures that observations from the Earth must occur at small elongation angles and be subject to the greatest amount of DCR.

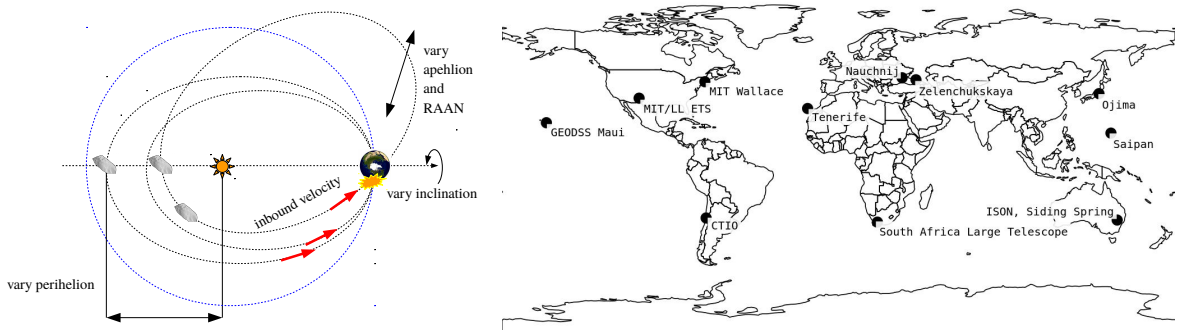

(a) Orbit geometry (b) Observing network

Figure 13: Simulated asteroid impact geometry and observing network. Earth-impacting orbits are simulated over all possible combinations of perihelion, aphelion, and orbital inclination such that an impact occurs as the asteroid approaches Earth from inside 1 AU, forcing observations of the approach to occur at high zenith distances.

The orbits that impact the Earth at a given point in time are constrained by the three-dimensional location of the Earth at the impact time, leaving three free parameters for the orbit: perihelion q, aphelion Q, and inclination i. We sample the free parameters to search for cases where DCR-induced observation error introduces a statistically significant bias in the impact point prediction. We consider the cases where $q \in [0.5, 0.9]$, $Q \in [1.0, 3.5]$ and $i \in [-40, 40]$.

We sample this space as follows. Given desired values of q, Q, and i, we select an impact date and compute a heliocentric Keplerian orbital state coincident with the Earth at the chosen time. Using two-body heliocentric physics, this initial state is propagated backward six months before impact. This becomes the seed state. The velocity component of the seed state is differentially corrected such that when propagated forward six months using the full JPL solar system force model, an Earth impact is achieved. The only criterion for terminating the differential correction is that the incoming velocity vector of the impact have an elevation angle above 45 degrees. We make this choice to avoid nonlinearities from the curvature of the Earth when using linear transformations to project state covariances of orbit estimates onto the surface of the Earth. We do not select specific aiming points on the Earth's surface.

Once the orbit is generated, observations are simulated over the six month period prior to impact from all stations in the observing network in Figure 13(b). The stations are assumed to have 100% weather availability past astronomical twilight, be able to detect the target down to an elevation angle of 7 degrees, and to generate astrometric observations at a cadence of once per second with a formal accuracy of 200 mas rms. To save computation time, the observations are simulated as normal points at half-hour intervals with formal covariance of $200 \text{ mas}/\sqrt{1800} = 4$ mas. We then inject S-type vs C-type DCR bias into the observations along the station-local vertical direction.

We acknowledge that these assumptions on station capability and availability are not necessarily realistic given the way real telescopes operate and that our impact trajectories and timelines are specifically chosen to highlight a worst-case scenario. However, it is fair to assume that in the event of a real-world scenario such as the one described here, ground-based telescopes observing at low elevation angles would dominate the astrometric observations of such a hazardous object in the months leading up to impact.

4.2 Impact Point and Uncertainty Calculation

Orbit estimates and formal covariances are generated using all biased observations and the resulting state estimate and covariance are propagated forward in time to compute the biased impact point. The performance metric in this scenario is the physical location of the true impact point on the surface of the Earth with respect to the biased estimate and its predicted uncertainty. The projection of the formal covariance of the state estimate onto the ground is made rigorously assuming that all observational errors are distributed as zero-mean Gaussians. The purpose of this analysis is to demonstrate that when observation errors are not zero-mean because of unaccounted-for DCR, the resulting impact point estimate and its rigorously modeled uncertainty differs from the true impact location by a statistically significant amount.

The projection of an inertial 6-DOF covariance into a two-dimensional error distribution on the Earth's surface is a three-step procedure, illustrated in Figure 14. In the process of fitting to simulated observations, a fit covariance matrix $\mathbf{\Sigma}_{\text{fit,epoch}}$ is computed, and in the process of propagating the fit solution $\mathbf{x}_{\text{fit,epoch}}$ to the impact time, we also propagate[42] a state transition matrix $\mathbf{\Phi}(t_{\text{impact}})$ such that

$$\mathbf{x}_{\text{impact,gcrf}} = \mathbf{\Phi}(t_{\text{impact}})\mathbf{x}_{\text{fit,epoch}} \tag{5}$$

This is in inertial coordinates, and we rotate into Earth-fixed coordinates via standard intertial-to-terrestrial transformations[43]

$$\mathbf{x}_{\text{impact,itrf}} = \begin{bmatrix} \mathbf{R}_{\text{gcrf2itrf}} & \mathbf{0} \\ \dot{\mathbf{R}}_{\text{gcrf2itrf}} & \mathbf{R}_{\text{gcrf2itrf}} \end{bmatrix} \mathbf{x}_{\text{impact,gcrf}} \tag{6}$$

Taken together, this implies that the covariance projected into Earth-fixed coordinates is given by

$$\mathbf{\Sigma}_{\text{itrf,impact}} = \begin{bmatrix} \mathbf{R}_{\text{gcrf2itrf}} & \mathbf{0} \\ \dot{\mathbf{R}}_{\text{gcrf2itrf}} & \mathbf{R}_{\text{gcrf2itrf}} \end{bmatrix} \mathbf{\Phi}(t_{\text{impact}})\mathbf{\Sigma}_{\text{fit,epoch}}\mathbf{\Phi}(t_{\text{impact}})^T \begin{bmatrix} \mathbf{R}_{\text{gcrf2itrf}} & \mathbf{0} \\ \dot{\mathbf{R}}_{\text{gcrf2itrf}} & \mathbf{R}_{\text{gcrf2itrf}} \end{bmatrix}^T \tag{7}$$

Next, it is necessary to collapse the Earth-fixed covariance to two dimensions along the inbound velocity vector. Figure 14(b) provides graphical intuition for why that is the case. The two-dimensional plane perpendicular to the velocity vector

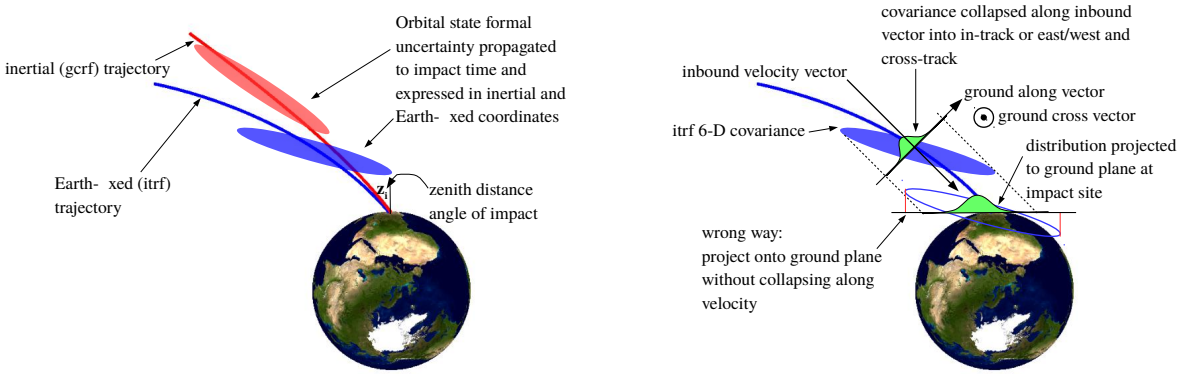

(a) Cartesian error at impact time (b) Collapsing along velocity and projecting on ground

Figure 14: Schematic of asteroid impact point uncertainty projection

is defined by along-track $\mathbf{a}$ and cross-track $\mathbf{c}$ directions as shown in Figure 14(b) and the collapse operation consists of

$$\mathbf{\Sigma}_{\text{AC,space}} = \begin{bmatrix} \mathbf{a}^T & \mathbf{0} \\ \mathbf{c}^T & \mathbf{0} \end{bmatrix} \mathbf{\Sigma}_{\text{itrf,impact}} \begin{bmatrix} \mathbf{a} & \mathbf{c} \\ \mathbf{0} & \mathbf{0} \end{bmatrix} \tag{8}$$

Lastly, the collapsed covariance is layed down on the surface of the Earth by a cosine projection

$$\mathbf{\Sigma}_{\text{AC,ground}} = \begin{bmatrix} \frac{1}{\cos z_i} & 0 \\ 0 & 1 \end{bmatrix} \mathbf{\Sigma}_{\text{AC,space}} \begin{bmatrix} \frac{1}{\cos z_i} & 0 \\ 0 & 1 \end{bmatrix} \tag{9}$$

where z_i is the zenith angle of the inbound trajectory in Earth-fixed coordinates.

The square root of the largest eigenvalue of $\mathbf{\Sigma}_{\text{AC,ground}}$ is quoted as the ground uncertainty of the impact point. This implicitly approximates the surface of the Earth as flat and neglects the curvature of the inbound trajectory near impact time, hence the initial selection of impact scenarios where the inbound velocity comes from low zenith distances to make linearization along that dominant eigenvector a valid operation. The dominant eigenvector generally aligns with the along-track direction. Cross-track errors are several orders of magnitude smaller than in-track error and are not considered.

4.3 Existence of Dangerous Cases

We define a dangerous case to be an instance where the separation between the true impact point and the biased estimate exceeds 200 km and exceeds the $\pm 3\sigma$ uncertainty bounds of the biased impact point in the along-track direction. We assume that a 30-day observation arc would be necessary to form an estimate of the impact point and search for cases where the timing of that 30-day arc subjects the observations to sufficient DCR bias to force such a dangerous scenario.

Consider the scenario where $Q = 1$, $q = 0.7$ and $i = 0$. The geometry of the asteroid's approach causes it to go between the Earth and sun prior to impact and this forces a strong coupling between the volume of data available and the amount of DCR imposed on that data in the months prior to impact. If discovery of the asteroid occurs 145 days before impact, the 30-day window will elapse 105 days before impact and the biased and unbiased impact points for the best available orbit estimate will be biased by a statistically significant amount relative to the uncertainty in the orbit fit.

The evolution of the bias and the fit uncertainty as a function of time and observation elevation cutoff is shown in the top panel of Figure 15 and the estimates possible at 105 days before impact are shown in the bottom panel. Data volume decreases with higher elevation cutoffs but data quality improves and the interplay is quite stark as the separation between true and biased impact points increases with progressively more data from low elevations but the uncertainty shrinks, leading to a potentially false sense of security in this worst-case scenario.

The existence of conditions where the true bias exceeds the formal error are not confined to the particular case of $Q = 1$, $q = 0.7$ and $i = 0$. Figure 16 shows the same scenario for an orbit like that of 3122 Florence with $Q = 2.5$, $q = 1.0$ and

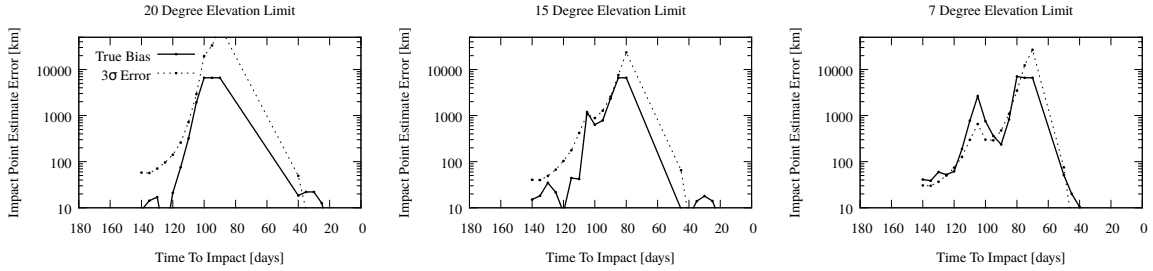

(a) Bias and uncertainty vs time and elevation limit

20° elevation limit 15° elevation limit 7° elevation limit

(b) True and biased impact points $\pm 3\sigma$ uncertainty 105 days before impact

Figure 15: Evolution of impact bias and uncertainty with time for $Q = 1$, $q = 0.7$ and $i = 0$. The true impact point bias from unaccounted-for DCR increases with progressively lower elevation cut-off. However, progressively lower elevation cutoffs drastically increase the data volume, thereby also lowering the formal error of the impact point estimate if DCR bias is not accounted for. The dangerous geometries correspond to the true bias trace exceeding the formal error trace.

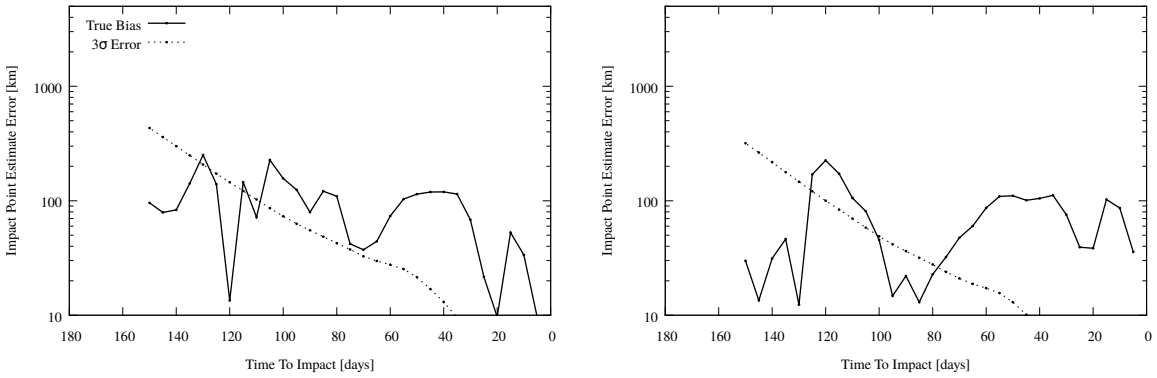

(a) $i = +20°$ (b) $i = -20°$

Figure 16: Evolution of impact bias and uncertainty with time for Florence-like orbit ($Q = 2.5$, $q = 1.0$ and $i = \pm 20°$). Calculations are for a rolling 30-day observation window with observation cadence 0.5 Hz from all stations in view down to a 7° elevation limit.

$i = \pm 20°$, where again there exist periods where the DCR bias in the observations does not attenuate and contributes to a statistically significant bias in the impact point. We find that these cases exist for nearly all choices of free parameters at some point within the six month window in our simulation.

5. CONCLUSION

5.1 Summary

We have demonstrated that differential color refraction is the dominant systematic error source in ground-based astrometry with modern star catalogs. This error source is target-dependent, and thus compensation requires spectroscopic characterization on a per-target basis. Using high-volume observations of GNSS satellites and archived observations of asteroids with known spectral types we have demonstrated that DCR bias exists in real data. Our targeted high-volume observations of 3122 Florence demonstrate that narrow band filters are not always a valid mitigation strategy against DCR and that care must be taken to compensate for stellar, as well as target, DCR bias. Spectroscopic measurements may be required to fully compensate for DCR on even seemingly well-characterized targets and we have derived resolution requirements for such spectroscopic measurements. The effect of uncompensated DCR bias on orbit estimation may not always attenuate with increased observation arc length and geometric diversity of observing stations. We have shown simulated cases where DCR bias compounds over time and resolves into a statistically significant impact point bias for hazardous asteroids.

5.2 Recommendations

Our demonstration of near-zero error in the horizontal residuals of observations of GPS and GLONASS satellites using recently-released star catalogs make a strong case for all astrometric observing programs to upgrade to the best-available astrometric star catalogs and implement stellar DCR compensation in their data reduction pipelines. We further recommend that all observing sites retain information on their optical configuration and DCR correction pipeline to enable after-the-fact compensation for DCR on asteroids whose spectra are measured at a later date. Lastly, we recommend spectroscopic characterization of all potentially hazardous asteroids at 10–20 nm resolution over the full silicon band and over a variety of phase angles to enable after-the-fact DCR compensation to already-collected astrometric observations. Where possible, we recommend that spectroscopic observations occur in concert with astrometric observations. We especially encourage simultaneous observations of flyby events where the target's proximity permits rapid high-SNR measurement of phase-dependent and surface temperature-dependent perturbations to its reflectance spectrum.

5.3 Future Work

Further validation of the atmospheric models used for DCR predictions require large data volumes to validate their accuracy with high confidence. The difficulty of having a good truth orbit on asteroids at the time of observation recommends that further DCR work be conducted on GNSS and ILRS satellite constellations. We are undertaking a spectroscopic observation campaign on active GPS and GLONASS satellites to enable validation of DCR compensation techniques.

While the unambiguous presence of DCR was shown with the high-volume observations of GPS satellites and 3122 Florence, the major uncertainty in the predictability of DCR was uncertainty in the DCR of fiducial stars. This ambiguity originates from the varying quality and quantity of photometry available in the URAT1 and UCAC5 catalogs which leads to uncertainty in estimating the amount of interstellar reddening in a star's detectable spectrum and thus its DCR with respect to the solar-analog baseline. The recent publication of Gaia DR2 containing parallax and interstellar extinction estimates for the majority of fiducial stars useful for ground-based astrometry will enable more rigorous estimation of stellar DCR. We expect improved performance over URAT1 and UCAC5 by incorporating Gaia parallaxes in DCR compensation. In concert with our planned spectroscopic observations of GNSS satellites, we will perform spot-check spectroscopic observations on representative star fields in order to validate with direct measurement the stellar spectra and DCR predictions derived from Gaia photometry and astrometry.

6. ACKNOWLEDGMENTS

The authors extend thanks to Mr. Dan Birchall, Mr. Matthew Blythe, and Mr. Greg Spitz of MIT Lincoln Laboratory and Mr. Tim Brothers and Dr. Michael Person of the MIT Earth and Planetary Science Department for supporting observations of 3122 Florence, Dr. J. Scott Stuart of MIT Lincoln Laboratory for providing insight into LINEAR, and Dr. Jon Giorgini of the Solar System Dynamics Group at the Jet Propulsion Laboratory for providing details of the Horizons force model.

This material is based upon work supported under Air Force Contract No. FA8721-05-C-0002. Any opinions, findings, conclusions or recommendations expressed in this material are those of the authors and do not necessarily reflect the views of the U.S. Government.

REFERENCES

[1] Gaia Collaboration, Brown, A. G. A., Vallenari, A., Prusti, T., de Bruijne, J. H. J., Mignard, F., Drimmel, R., Babusiaux, C., Bailer-Jones, C. A. L., Bastian, U., and et al., "Gaia Data Release 1. Summary of the astrometric, photometric, and survey properties," *Astronomy & Astrophysics* **595**, A2 (Nov. 2016).

[2] "IAU Minor Planet Center." `http://www.minorplanetcenter.net`. Accessed: 2017-10-30.

[3] Stokes, G. H., Evans, J. B., Viggh, H. E. M., Shelly, F. C., and Pearce, E. C., "Lincoln Near-Earth Asteroid Program (LINEAR)," *Icarus* **148**, 21–28 (Nov. 2000).

[4] Filippenko, A. V., "The importance of atmospheric differential refraction in spectrophotometry," *PASP* **94**, 715–721 (Aug. 1982).

[5] Stone, R. C., "The effect of differential color refraction on declinations determined in meridian circle programs," *Astronomy & Astrophysics* **138**, 275–284 (Sept. 1984).

[6] Auer, L. H. and Standish, E. M., "Astronomical Refraction: Computational Method for All Zenith Angles," *The Astronomical Journal* **119**, 2472–2474 (May 2000).

[7] Berk, A., Anderson, G. P., Acharya, P. K., Bernstein, L. S., Muratov, L., Lee, J., Fox, M. J., Adler-Golden, S. M., Chetwynd, Jr., J. H., Hoke, M. L., Lockwood, R. B., Gardner, J. A., Cooley, T. W., and Lewis, P. E., "MODTRAN5: a reformulated atmospheric band model with auxiliary species and practical multiple scattering options," in [*Algorithms and Technologies for Multispectral, Hyperspectral, and Ultraspectral Imagery X*], Shen, S. S. and Lewis, P. E., eds., *Proc. SPIE* **5425**, 341–347 (Aug. 2004).

[8] Smith, D., Shiles, E., and Inokuti, M., "The optical properties of metallic aluminum," in [*Handbook of Optical Constants of Solids*], Palik, E. D., ed., 369 – 406, Academic Press, Burlington (1997).

[9] Malitson, I. H., "Interspecimen comparison of the refractive index of fused silica," *J. Opt. Soc. Am.* **55**, 1205–1209 (Oct 1965).

[10] Jorden, P. R., Jordan, D., Jerram, P. A., Pratlong, J., and Swindells, I., "e2v new CCD and CMOS technology developments for astronomical sensors," in [*High Energy, Optical, and Infrared Detectors for Astronomy VI*], **9154**, 91540M, International Society for Optics and Photonics (2014).

[11] Cardelli, J. A., Clayton, G. C., and Mathis, J. S., "The relationship between infrared, optical, and ultraviolet extinction," *Astrophysical Journal* **345**, 245–256 (Oct. 1989).

[12] Pickles, A. J., "A Stellar Spectral Flux Library: 1150-25000 Å," *PASP* **110**, 863–878 (July 1998).

[13] Sekiguchi, M. and Fukugita, M., "A Study of the B-V Color-Temperature Relation," *The Astronomical Journal* **120**, 1072–1084 (Aug. 2000).

[14] Chapman, C. R. and Gaffey, M. J., [*Reflectance spectra for 277 asteroids*], 655–687 (1979).

[15] Bus, S. J. and Binzel, R. P., "Phase II of the Small Main-Belt Asteroid Spectroscopic Survey. A Feature-Based Taxonomy," *Icarus* **158**, 146–177 (July 2002).

[16] Binzel, R. P., Rivkin, A. S., Stuart, J., Harris, A. W., Bus, S. J., and Burbine, T. H., "Observed spectral properties of near-earth objects: results for population distribution, source regions, and space weathering processes," *Icarus* **170**(2), 259 – 294 (2004).

[17] DeMeo, F. E., Binzel, R. P., Slivan, S. M., and Bus, S. J., "An extension of the Bus asteroid taxonomy into the near-infrared," *Icarus* **202**, 160–180 (July 2009).

[18] Tholen, D. J. and Barucci, M. A., "Asteroid taxonomy," in [*Asteroids II*], Binzel, R. P., Gehrels, T., and Matthews, M. S., eds., 298–315 (1989).

[19] Monet, D. G., Levine, S. E., Canzian, B., Ables, H. D., Bird, A. R., Dahn, C. C., Guetter, H. H., Harris, H. C., Henden, A. A., and Leggett, S. K., "The USNO-B catalog," *The Astronomical Journal* **125**(2), 984 (2003).

[20] ESA, ed., [*The HIPPARCOS and TYCHO catalogues. Astrometric and photometric star catalogues derived from the ESA HIPPARCOS Space Astrometry Mission*], *ESA Special Publication* **1200** (1997).

[21] Zacharias, N., Finch, C., Girard, T., Hambly, N., Wycoff, G., Zacharias, M. I., Castillo, D., Corbin, T., DiVittorio, M., Dutta, S., Gaume, R., Gauss, S., Germain, M., Hall, D., Hartkopf, W., Hsu, D., Holdenried, E., Makarov, V., Martinez, M., Mason, B., Monet, D., Rafferty, T., Rhodes, A., Siemers, T., Smith, D., Tilleman, T., Urban, S., Wieder, G., Winter, L., and Young, A., "The Third US Naval Observatory CCD Astrograph Catalog (UCAC3)," *The Astronomical Journal* **139**, 2184–2199 (June 2010).

[22] Zacharias, N., Finch, C. T., Girard, T. M., Henden, A., Bartlett, J. L., Monet, D. G., and Zacharias, M. I., "The Fourth US Naval Observatory CCD Astrograph Catalog (UCAC4)," *The Astronomical Journal* **145**, 44 (Feb. 2013).

[23] Zacharias, N., Finch, C., Subasavage, J., Bredthauer, G., Crockett, C., Divittorio, M., Ferguson, E., Harris, F., Harris, H., Henden, A., Kilian, C., Munn, J., Rafferty, T., Rhodes, A., Schultheiss, M., Tilleman, T., and Wieder, G., "The first U.S. Naval Observatory robotic astrometric telescope catalog," *The Astronomical Journal* **150**(4), 101 (2015).

[24] Lindegren, L., Lammers, U., Bastian, U., Hernández, J., Klioner, S., Hobbs, D., Bombrun, A., Michalik, D., Ramos-Lerate, M., Butkevich, A., Comoretto, G., Joliet, E., Holl, B., Hutton, A., Parsons, P., Steidelmüller, H., Abbas, U., Altmann, M., Andrei, A., Anton, S., Bach, N., Barache, C., Becciani, U., Berthier, J., Bianchi, L., Biermann, M., Bouquillon, S., Bourda, G., Brüsemeister, T., Bucciarelli, B., Busonero, D., Carlucci, T., Castañeda, J., Charlot, P., Clotet, M., Crosta, M., Davidson, M., de Felice, F., Drimmel, R., Fabricius, C., Fienga, A., Figueras, F., Fraile, E., Gai, M., Garralda, N., Geyer, R., González-Vidal, J. J., Guerra, R., Hambly, N. C., Hauser, M., Jordan, S., Lattanzi, M. G., Lenhardt, H., Liao, S., Löffler, W., McMillan, P. J., Mignard, F., Mora, A., Morbidelli, R., Portell, J., Riva, A., Sarasso, M., Serraller, I., Siddiqui, H., Smart, R., Spagna, A., Stampa, U., Steele, I., Taris, F.,

Torra, J., van Reeven, W., Vecchiato, A., Zschocke, S., de Bruijne, J., Gracia, G., Raison, F., Lister, T., Marchant, J., Messineo, R., Soffel, M., Osorio, J., de Torres, A., and O'Mullane, W., "Gaia Data Release 1. Astrometry: one billion positions, two million proper motions and parallaxes," *Astronomy & Astrophysics* **595**, A4 (Nov. 2016).
[25] Zacharias, N., Finch, C., and Frouard, J., "UCAC5: New proper motions using Gaia DR1," *The Astronomical Journal* **153**(4), 166 (2017).
[26] Gubler, J. and Tytler, D., "Differential Atmospheric Refraction and Limitations on the Relative Astrometric Accuracy of Large Telescopes," *PASP* **110**, 738–746 (June 1998).
[27] Altmann, M., Bouquillon, S., Taris, F., Steele, I. A., Smart, R. L., Andrei, A. H., Barache, C., Carlucci, T., and Els, S. G., "GBOT: ground based optical tracking of the Gaia satellite," in [*Observatory Operations: Strategies, Processes, and Systems V*], *Proc. SPIE* **9149**, 91490P (Aug. 2014).
[28] Carpino, M., Milani, A., and Chesley, S. R., "Error statistics of asteroid optical astrometric observations," *Icarus* **166**(2), 248 – 270 (2003).
[29] Shao, M., Nemati, B., Zhai, C., Turyshev, S. G., Sandhu, J., Hallinan, G., and Harding, L. K., "Finding very small near-earth asteroids using synthetic tracking," *The Astrophysical Journal* **782**(1), 1 (2014).
[30] Zhai, C., Shao, M., Nemati, B., Werne, T., Zhou, H., Turyshev, S. G., Sandhu, J., Hallinan, G., and Harding, L. K., "Detection of a faint fast-moving near-earth asteroid using the synthetic tracking technique," *The Astrophysical Journal* **792**(1), 60 (2014).
[31] Farnocchia, D., Chesley, S., Chamberlin, A., and Tholen, D., "Star catalog position and proper motion corrections in asteroid astrometry," *Icarus* **245**, 94 – 111 (2015).
[32] "Annual report," tech. rep., MIT Lincoln Laboratory, 244 Wood Street, Lexington MA, 02421 (2010).
[33] Dow, J. M., Neilan, R. E., and Rizos, C., "The International GNSS Service in a changing landscape of Global Navigation Satellite Systems," *Journal of Geodesy* **83**(3), 191–198 (2009).
[34] Schaefer, B. E. and Liller, W., "Refraction near the horizon," *PASP* **102**, 796–805 (July 1990).
[35] "JPL Horizons." `https://ssd.jpl.nasa.gov/horizons.cgi`. Accessed: 2017-10-30.
[36] Moyer, T., [*Formulation for Observed and Computed Values of Deep Space Network Data Types for Navigation*], JPL Deep-Space Communications and Navigation Series, Wiley (2005).
[37] Sanchez, J. A., Reddy, V., Nathues, A., Cloutis, E. A., Mann, P., and Hiesinger, H., "Phase reddening on near-earth asteroids: Implications for mineralogical analysis, space weathering and taxonomic classification," *Icarus* **220**(1), 36 – 50 (2012).
[38] Thomas, C. A., Emery, J. P., Trilling, D. E., Delb, M., Hora, J. L., and Mueller, M., "Physical characterization of warm spitzer-observed near-earth objects," *Icarus* **228**(Supplement C), 217 – 246 (2014).
[39] Fukugita, M., Ichikawa, T., Gunn, J. E., Doi, M., Shimasaku, K., and Schneider, D. P., "The Sloan Digital Sky Survey Photometric System," *The Astronomical Journal* **111**, 1748 (Apr. 1996).
[40] Vilas, F. and Gaffey, M. J., "Phyllosilicate absorption features in main-belt and outer-belt asteroid reflectance spectra," *Science* **246**, 790–792 (Nov. 1989).
[41] Burbine, T., [*Asteroids: Astronomical and Geological Bodies*], Cambridge University Press (2016).
[42] Montenbruck, O. and Gill, E., [*Satellite Orbits: Models, Methods, and Applications*], Physics and astronomy online library, Springer Berlin Heidelberg (2000).
[43] Urban, S. and Seidelmann, P., [*Explanatory Supplement to the Astronomical Almanac*], University Science Books (2013).